Article

Global satellite-observed daily vertical migrations of ocean animals

https://doi.org/10.1038/s41586-019-1796-9

Received: 27 September 2018

Accepted: 10 October 2019

Published online: 27 November 2019

Michael J. Behrenfeld[1]*, Peter Gaube[2], Alice Della Penna[2,3], Robert T. O'Malley[1], William J. Burt[4,5], Yongxiang Hu[6], Paula S. Bontempi[7], Deborah K. Steinberg[8], Emmanuel S. Boss[9], David A. Siegel[10,11], Chris A. Hostetler[6], Philippe D. Tortell[4,12] & Scott C. Doney[13]

Every night across the world's oceans, numerous marine animals arrive at the surface of the ocean to feed on plankton after an upward migration of hundreds of metres. Just before sunrise, this migration is reversed and the animals return to their daytime residence in the dark mesopelagic zone (at a depth of 200–1,000 m). This daily excursion, referred to as diel vertical migration (DVM), is thought of primarily as an adaptation to avoid visual predators in the sunlit surface layer[1,2] and was first recorded using ship-net hauls nearly 200 years ago[3]. Nowadays, DVMs are routinely recorded by ship-mounted acoustic systems (for example, acoustic Doppler current profilers). These data show that night-time arrival and departure times are highly conserved across ocean regions[4] and that daytime descent depths increase with water clarity[4,5], indicating that animals have faster swimming speeds in clearer waters[4]. However, after decades of acoustic measurements, vast ocean areas remain unsampled and places for which data are available typically provide information for only a few months, resulting in an incomplete understanding of DVMs. Addressing this issue is important, because DVMs have a crucial role in global ocean biogeochemistry. Night-time feeding at the surface and daytime metabolism of this food at depth provide an efficient pathway for carbon and nutrient export[6–8]. Here we use observations from a satellite-mounted light-detection-and-ranging (lidar) instrument to describe global distributions of an optical signal from DVM animals that arrive in the surface ocean at night. Our findings reveal that these animals generally constitute a greater fraction of total plankton abundance in the clear subtropical gyres, consistent with the idea that the avoidance of visual predators is an important life strategy in these regions. Total DVM biomass, on the other hand, is higher in more productive regions in which the availability of food is increased. Furthermore, the 10-year satellite record reveals significant temporal trends in DVM biomass and correlated variations in DVM biomass and surface productivity. These results provide a detailed view of DVM activities globally and a path for refining the quantification of their biogeochemical importance.

For decades, airplane-mounted lidar instruments have used the backscattering of light (bbp) from phytoplankton, zooplankton and small fish to locally map the distribution of these organisms in the water column[9–11]. In contrast to passive ocean sensors that measure reflected sunlight, lidar uses lasers as a light source and thus has the capacity to measure marine organisms both during the day and at night. When DVM animals are prominent, their nocturnal invasion of the surface ocean is expected to increase bbp at night compared with what the bbp would be in the absence of these animals. Five ship-based examples[12] of this DVM signature are shown in Fig. 1a, in which the animal signals contribute 7–28% of total night-time bbp. These signals appear as large spikes in this record because DVM animals are 'bright' targets

[1]Department of Botany and Plant Pathology, Oregon State University, Corvallis, OR, USA. [2]Applied Physics Laboratory, Air-Sea Interaction and Remote Sensing Department, University of Washington, Seattle, WA, USA. [3]Laboratoire des Sciences de l'Environnement Marin (LEMAR), UMR 6539 CNRS-Ifremer-IRD-UBO-Institut Universitaire Européen de la Mer (IUEM), Plouzané, France. [4]Earth, Ocean and Atmospheric Sciences, University of British Columbia, Vancouver, British Columbia, Canada. [5]College of Fisheries and Ocean Sciences, University of Alaska Fairbanks, Fairbanks, AK, USA. [6]NASA Langley Research Center, Hampton, VA, USA. [7]Earth Science Division, Science Mission Directorate, National Aeronautics and Space Administration Headquarters, Washington, DC, USA. [8]Virginia Institute of Marine Science, College of William & Mary, Gloucester Point, VA, USA. [9]School of Marine Sciences, University of Maine, Orono, ME, USA. [10]Earth Research Institute, University of California Santa Barbara, Santa Barbara, CA, USA. [11]Department of Geography, University of California Santa Barbara, Santa Barbara, CA, USA. [12]Botany Department, University of British Columbia, Vancouver, British Columbia, Canada. [13]Department of Environmental Sciences, University of Virginia, Charlottesville, VA, USA. *e-mail: mjb@science.oregonstate.edu

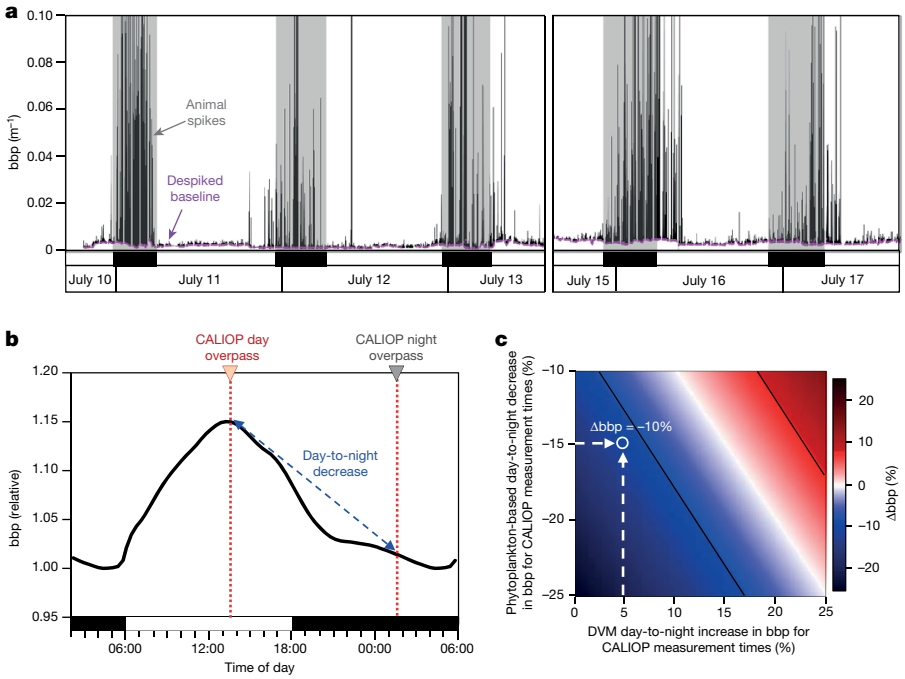

Fig. 1 | Marine animal and phytoplankton influences on day-to-night changes in particulate backscattering coefficients and the biomass-normalized difference ratio. a, Ship-based time-series of bbp showing nocturnal spikes associated with DVM animals and the general lack of these spikes during the day[12] (Methods). Black line, complete bbp record. Purple line, despiked baseline bbp record. **b**, Typical diel cycle in bbp of phytoplankton[19] (Methods). Red dotted line, daily equator crossing times of CALIOP. **a**, **b**, Black and white bars on the *x* axis indicate night and day, respectively. **c**, Biomass-normalized difference ratios (Δbbp) for ranges in DVM (*x* axis) and phytoplankton (*y* axis) contributions to day-to-night bbp changes. For example, if the phytoplankton diel cycle corresponds (as in **b**) to a 15% day-to-night decrease in bbp at the two CALIOP measurement times (horizontal white dashed arrow) and this decrease is countered by a 5% increase in bbp from DVM animals (vertical white dashed arrow), then Δbbp will have a value of −10% (colour inside labelled white circle). Diagonal black lines correspond to the colour bar range for the CALIOP observations shown in Fig. 2. Note that values on the *y* axis encompass the range of values expected in the PSO (Extended Data Fig. 5 and Supplementary Discussion).

compared to the phytoplankton and other suspended particles that constitute the much lower bbp baseline[13] (Fig. 1a); however, animals are also rarer and only occasionally pass through the small sample volume (around 2 ml) of the ship's bbp instrument. By contrast, a lidar with a much larger sampling volume can effectively capture the signal of all scattering components with every measurement. The satellite cloud–aerosol lidar with orthogonal polarization (CALIOP) sensor has been conducting such measurements for more than a decade[14,15] (Methods) and its bbp retrievals provide an opportunity to decipher global patterns in vertically migrating animals.

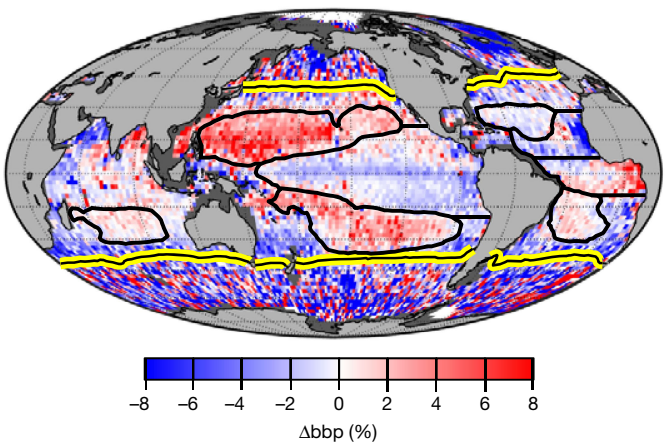

Fig. 2 | Global climatological signal of vertically migrating animals quantified as the normalized difference ratio. Data are 2° × 2° bin means for the 2008–2017 CALIOP record. Yellow-and-black line, contour of annual mean sea surface temperature of 15 °C, which effectively separates high-latitude seasonal seas from lower-latitude permanently stratified oceans[29,30]. Thick black lines separate major regions of the PSO (Fig. 3), in which the 5 subtropical gyres are defined by annual mean surface chlorophyll concentrations of ≤0.08 mg m^{-3}. Dark grey, excluded pixels in which the water column depth is less than 1,000 m.

The laser footprint of CALIOP has a diameter of 100 m at the ocean surface and a vertical sampling depth of 22 m in water. What this means is that each CALIOP measurement integrates the bbp signal from a water volume of 1.73×10^5 m^3, which is approximately 5×10^6 greater than the entire water volume measured over a given night in the field data shown in Fig. 1a. The large sampling volume of CALIOP thus ensures that each retrieved bbp value encompasses both the animals and suspended cells and particles in the surface layer. CALIOP is a polar orbiting sensor that conducts daytime and night-time (around 13:40 and 01:40 local time, respectively) near-nadir backscattering measurements along its orbit track at a sampling frequency that is equivalent to every 330 m on the ground. A slightly precessing orbit with a 16-day repeat cycle provides global bbp coverage, but ground tracks oriented in opposite directions on the light and dark sides of Earth mean that day and night bbp samples are rarely spatially coincident within a given 24 h period (Extended Data Fig. 1 and Supplementary Discussion). The global signature of DVM animals was therefore investigated by creating 2° × 2° (latitude by longitude) binned monthly CALIOP daytime (bbp^{day}) and night-time (bbp^{night}) values of bbp.

In the absence of any DVM, the biomass-normalized bbp difference ratio (equation (1)) is expected to yield a negative value for the measurement times of CALIOP (Fig. 1b):

$$\Delta bbp = (bbp^{night} - bbp^{day})/bbp^{day} \quad (1)$$

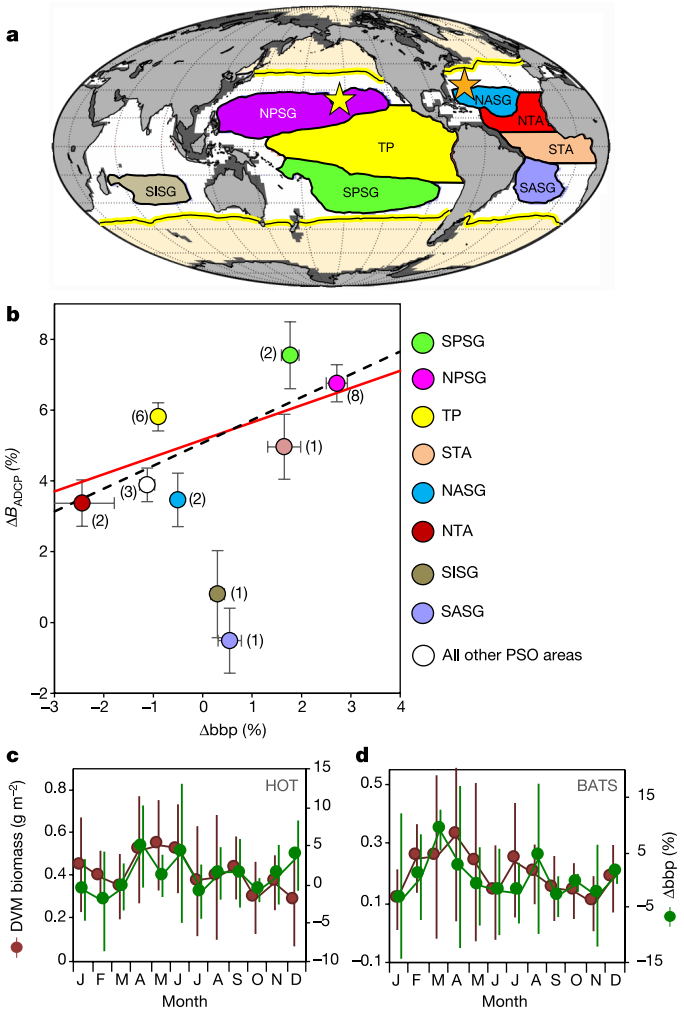

Fig. 3 | Comparison of CALIOP normalized difference ratios and field-based DVM measurements in the PSO. a, Colour-coded regions of the PSO from Fig. 2. Yellow star, location of the HOT site. Orange star, location of the BATS site. **b**, CALIOP (Δbbp) versus field ADCP (ΔB_{ADCP}) normalized difference ratios. Red line, two-sided least-squares linear regression fit to all 5° × 5° bins within our 8 PSO regions (slope = 0.42; *F*-test, $P = 0.001$, $n = 331$ independent geographical bins) (Extended Data Figs. 7, 8 and Supplementary Discussion). Symbols, regional mean values of Δbbp and ΔB_{ADCP}, with s.e.m. shown for each region (SISG, $n = 19$; SASG, $n = 18$; TP, $n = 115$; NASG, $n = 16$; NTA, $n = 23$; NPSG, $n = 59$; STA, $n = 22$; SPSG, $n = 59$; other, 302). For completeness, the mean value for all PSO bins outside our eight primary regions is indicated by the white symbol. Numbers next to each symbol indicate the median number of days with ADCP data within the 32-year field record for the bins within a given region. The dashed line indicates the two-sided least-squares linear regression fit to regionally averaged data for the $n = 6$ primary regions in which ΔB_{ADCP} is significantly greater than zero (TP, NASG, NTA, NPSG, STA and SPSG) (slope = 0.64, $r^2 = 0.55$, $P = 0.09$). **c**, Mean monthly field-measured (1994–2005)[21] migratory zooplankton biomass (g dry weight m^{-2}) for the HOT site (Methods) ($n = 112$ net haul samples) and CALIOP-measured Δbbp (2008–2017) ($n = 75$ monthly retrievals) for a 2° × 2° bin centred on the HOT site. Vertical lines indicate 1 s.d. Field and CALIOP data are offset on the *x* axis by 6 days to separate s.d. lines. **d**, As in **c**, for field (1994–2017) ($n = 285$ net haul samples) and CALIOP ($n = 87$ monthly retrievals) data for the BATS site.

This is because daytime increases in phytoplankton cell size and organic carbon content and night-time cell division and metabolism[16–18] create a baseline diel cycle in biomass-normalized bbp with an afternoon maximum and night-time minimum[19] (Fig. 1b and Extended Data Fig. 9). The presence of DVM animals increases bbp^{night} (Fig. 1a) and therefore causes Δbbp to become less negative than the phytoplankton-only signal or even positive if the migrating animals are sufficiently abundant. Thus, phytoplankton and DVM animals together determine Δbbp (Fig. 1c), in which the magnitude and sign of Δbbp is an index of the DVM signal strength relative to that of the phytoplankton.

The 2008–2017 CALIOP record reveals eight broad regions at tropical and subtropical latitudes (equatorward of the yellow-and-black lines in Fig. 2) where climatological mean Δbbp values are spatially coherent. In these regions, plankton populations are relatively stable over time as the water column is permanently stratified within the euphotic zone (referred to hereafter as the permanently stratified ocean (PSO)). These eight broad features (Fig. 2) correspond to the seasonally varying boundaries of the North Pacific (NPSG), South Pacific (SPSG), North Atlantic (NASG), South Atlantic (SASG) and South Indian (SISG) subtropical gyres, and the higher-nutrient tropical Pacific (TP), north tropical (NTA) and south tropical (STA) Atlantic (Figs. 2, 3a and Extended Data Fig. 2). Within these regions, Δbbp values are persistently positive in the NPSG, persistently negative in the TP and NTA, and strongly seasonal in the NASG, STA and all three Pacific areas (Extended Data Fig. 3). In the high-latitude seasonal regions (poleward of the yellow-and-black line in Fig. 2), the CALIOP record reveals large climatological mean values for Δbbp. However, persistent cloud cover and small-scale spatiotemporal variations in plankton populations in these regions cause within-bin mismatches in bbp^{day} and bbp^{night} data that yield significant bin-to-bin variability in Δbbp (Supplementary Discussion). From this point forward, therefore, our analysis primarily focuses on the eight regions of the PSO.

If variability in Δbbp is mostly a reflection of the strength of the DVM rather than changes in the phytoplankton cycle, then results shown in Fig. 2 suggest that there are significant regional differences in the relative night-time abundance of these animals. To test this DVM-basis of the regional patterns, we compared CALIOP data to historical field acoustic Doppler current profiler (ADCP) observations of paired day (I_{dB}^{day}) and night (I_{dB}^{night}) acoustic backscatter. Owing to the sparsity of such data, it was necessary to aggregate 32 years (1985–2017) of field measurements into monthly 5° × 5° bins to achieve reasonable global coverage (Methods). We then calculated median values of the normalized difference ratio:

$$\Delta B_{ADCP} = (I_{dB}^{night} - I_{dB}^{day})/I_{dB}^{day} \quad (2)$$

CALIOP bbp data were then reaggregated into equivalent 5° × 5° bins and regional median values of Δbbp were calculated using only those calendar months and bins for which ADCP data were available. Comparison of ΔB_{ADCP} and Δbbp for all bins within our eight PSO regions yielded a statistically significant relationship ($P = 0.001$, $n = 331$) (Fig. 3b) with a slope that is very similar to that calculated from regionally averaged values for the six regions in which ADCP data identify a significant DVM signal (Fig. 3b and Supplementary Discussion). In other words, the ADCP and lidar datasets both indicate that DVM animals constitute a greater fraction of night-time plankton communities in the optically clear subtropical gyres that are most advantageous to visual predators. Notably, the regionally averaged data for the SISG and SASG deviate from the other PSO regions (Fig. 3b). The reason for this difference is unknown. These are the only two regions in which ΔB_{ADCP} is near zero, suggesting either that there are few DVM animals or that the influx of night-time DVM animals is compensated by reverse-DVM animals that leave the surface layer[20]. By contrast, CALIOP data indicate that there is a moderate DVM signal in the SISG and SASG (Fig. 3b). Perhaps the discrepancy in these two regions is simply due to poor ADCP coverage (typically one day–night observation per 5° × 5° bin for the 32-year field record). However, all of the ADCP data in the SASG and all but eight observations in the SISG predate the CALIOP mission, so a temporal change in DVM populations cannot be ruled out.

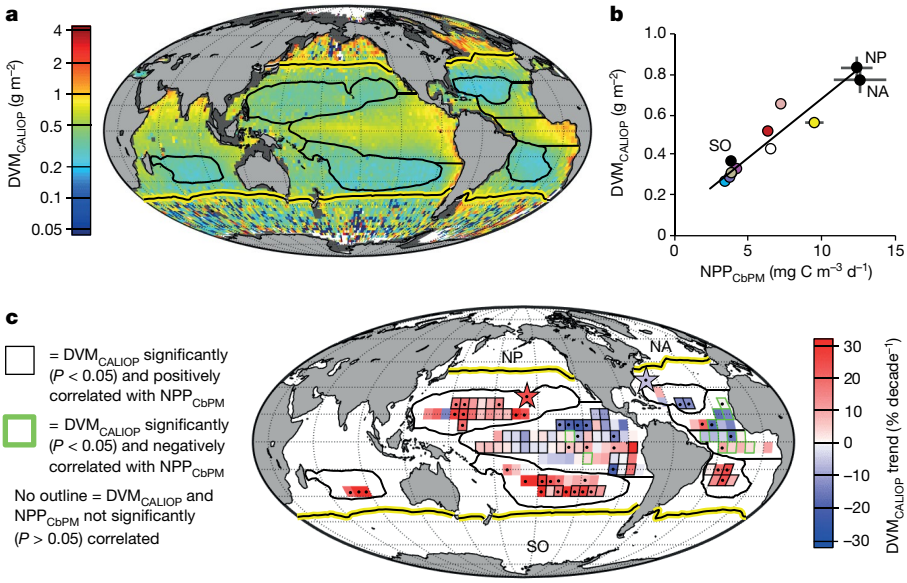

Fig. 4 | CALIOP-based estimates of vertically migrating animal biomass (DVM$_{CALIOP}$) and temporal changes. a, Annual mean DVM$_{CALIOP}$ (g dry weight m^{-2}). Yellow-and-black and thick black lines as in Fig. 2. **b**, Relationship between annual mean regional DVM$_{CALIOP}$ and mixed-layer net primary production data from the carbon-based production model (NPP$_{CbPM}$; mg C m^{-3} day^{-1}) (Methods). Solid line, two-sided least-squares linear regression fit (r^2 = 0.80; F-test, P = 0.002, n = 9 geographical regions) of the PSO regions, which are colour-coded according to Fig. 3a. Black symbols, high-latitude North Pacific (NP), North Atlantic (NA) and Southern Ocean (SO) (see **c**). Horizontal and vertical lines indicate 1 s.d. for annual values between 2008 and 2017 (n = 111 months per geographical region). **c**, Rate of change in DVM$_{CALIOP}$ for 6° × 6° bins for eight PSO regions and at the HOT and BATS sites (coloured stars). Only bins that stay within their respective regional boundaries throughout the year are shown (Extended Data Fig. 2). A black dot in centre of bin indicates that the trend is significant (two-sided least-squares linear regression; F-test, P < 0.05, n = 111 months per bin). Outlined bins exhibit a significant (two-sided least-squares linear regression; F-test P < 0.05, n = 111 months per bin) relationship between DVM$_{CALIOP}$ and NPP$_{CbPM}$, with black and green outlines indicating positive and negative correlations, respectively.

Day and night zooplankton net tows provide quantitative field measurements of DVM biomass, but these labour-intensive measurements are rarely collected at regular intervals over long periods. Two exceptions in the PSO are the sustained records at the Hawaii ocean time-series (HOT) site (22° 45′ N, 158° W)[21] and the Bermuda Atlantic time-series (BATS) site (31° 40′ N, 64° 10′ W)[22] (Fig. 3a). Despite considerable interannual variability, significant (P < 0.01) seasonal cycles in DVM biomass (g dry weight m^{-2}) are observed at these locations. For the CALIOP bin centred on the HOT site, the seasonal cycle in Δbbp from January to November is significantly correlated (r^2 = 0.44, P = 0.03) with field observations (Fig. 3c). Similarly, Δbbp for the CALIOP bin centred on the BATS site exhibits a two-peaked seasonal cycle that correlates well with field observations from August to June (r^2 = 0.42, P = 0.03) (Fig. 3d). These results are of particular note given the temporal and spatial contrast between datasets (CALIOP data are from 2° × 2° bins collected from 2008 to 2017; zooplankton net data were collected at HOT and BATS from 1994 to 2005[21] and from 1994 to 2017, respectively). Thus, the correspondence between Δbbp (which includes DVM animals, surface-resident organisms and suspended particles) and animal-specific ADCP[22] (Fig. 3b) and net measurements (Fig. 3c, d) gives confidence to the DVM signal detected by CALIOP.

The biomass-normalized Δbbp property reflects the relative strength of the DVM signal, whereas DVM biomass (DVM$_{CALIOP}$) is more quantitatively related to the simple difference, bbp^{night} − bbp^{day}. We estimated DVM$_{CALIOP}$ from this difference as:

$$\mathrm{DVM}_{CALIOP} = a(\mathrm{bbp}^{night} - c\mathrm{bbp}^{day}) \quad (3)$$

in which a is an empirical conversion factor between backscattering (m^{-1}) and biomass (g m^{-2}) determined from BATS and CALIOP data and c accounts for night–day differences in bbp from growth-rate- and day-length-dependent variations in the diel cycle of phytoplankton (Methods). Application of equation (3) to the CALIOP record yields a global distribution of DVM$_{CALIOP}$ (Fig. 4a) that differs markedly from Δbbp (Fig. 2). In particular, DVM$_{CALIOP}$ is generally low in the subtropical gyres and high in the nutrient-enriched tropical regions. Therefore, although the relative contribution of DVM animals to night-time plankton communities is higher in clearer waters (Fig. 2), total DVM biomass is higher in more productive regions in which there is a greater availability of food (Fig. 4a). Indeed, the annual mean DVM$_{CALIOP}$ for our PSO regions is highly correlated with passive ocean-colour-based estimates of net primary production (r^2 = 0.80, P = 0.002) (Fig. 4b, Methods). Results for the high-latitude northern and southern regions are also consistent with this finding (Fig. 4b). Notably, an increase in phytoplankton production yields a less than proportional increase in DVM$_{CALIOP}$, as might be expected for migrating animals that may be multiple trophic levels removed from the phytoplankton. Consequently, the night–day difference in bbp caused by the diel cycle of phytoplankton (Fig. 1b) generally increases more rapidly than the DVM signal as productivity increases, resulting in negative Δbbp values in productive tropical regions (Fig. 2).

Evidence of long-term changes in zooplankton populations, often linked to climate oscillations, has emerged from field time-series studies[22–27]. At the HOT site, field-measured DVM zooplankton biomass increased on average by 12.4 mg m^{-2} year^{-1} (38% per decade) between 1994 and 2005 (P = 0.04)[21]. The DVM$_{CALIOP}$ record indicates that this trend continued (P = 0.05) at a rate of 23% per decade from 2008 to 2017 (Fig. 4c). At BATS, an overall increasing trend of 7.4 mg m^{-2} year^{-1} (54% per decade) was reported for field observations from 1994 to 2011 (P < 0.01)[22]. Expanding this dataset to 2017 and re-evaluating the data, we find that DVM biomass increased 63% per decade from 1994 to 2007 (P = 0.01) and then decreased 28% per decade from 2008 to 2017 (P = 0.04). For this latter period, DVM$_{CALIOP}$ data similarly suggest a decreasing trend (9% per decade; P > 0.1) for the 2° × 2° bin that encompasses the BATS site (Fig. 4c). The global coverage provided by CALIOP now allows the evaluation of DVM biomass temporal trends

to be greatly expanded. For example, subdividing our 8 PSO regions (Fig. 3a) into 6° × 6° bins and evaluating only those bins that remain within their respective regional boundaries throughout the year (Extended Data Fig. 2) reveals that decadal trends in DVM_{CALIOP} have coherent geographical patterns (Fig. 4c). Specifically, a predominance of increasing DVM animal biomass is observed in the NPSG, SPSG, SASG and SISG, whereas decreasing DVM biomass is indicated across much of the tropical regions and the NASG. Moreover, DVM_{CALIOP} is positively correlated with changes in phytoplankton production for most bins, but in the two tropical Atlantic regions the correlations are counter-intuitively inverse (Fig. 4c).

The power of a satellite lidar when studying marine animals lies in its unparalleled annual coverage of the global ocean. By contrast, in this study, it was necessary to compile more than 30 years of ADCP measurements to create a single field-test dataset, and even then spatial and temporal coverage remained poor in many regions (Extended Data Fig. 4). A challenge with satellite lidar data, however, is that the measured night–day bbp differences are not solely owing to DVM animals, so continued work is needed to refine descriptions of the non-DVM contributors (Methods and Supplementary Discussion). Further analyses of field data (for example, ADCP data or continuous plankton recorder survey observations) and modelling[28] are needed to fully understand the causative ecological processes that underlie the spatial and temporal DVM patterns that are observed from space, and an advanced satellite lidar with ocean-profiling capabilities[11] may contribute new insights into DVM behaviours (Supplementary Discussion). Although there are multiple new avenues to pursue regarding the study of DVM animals, the results presented here provide a step forward in the global exploration of this greatest animal migration on Earth.

Online content

Any methods, additional references, Nature Research reporting summaries, source data, extended data, supplementary information, acknowledgements, peer review information; details of author contributions and competing interests; and statements of data and code availability are available at https://doi.org/10.1038/s41586-019-1796-9.

1. Lampert, W. The adaptive significance of diel vertical migration of zooplankton. *Funct. Ecol.* **3**, 21–27 (1989).
2. Hays, G. C. A review of the adaptive significance and ecosystem consequences of zooplankton diel vertical migrations. *Hydrobiologia* **503**, 163–170 (2003).
3. Cuvier, G. *Le Règne Animal distribué d'après son Organisation pour à l'Histoire Naturelle des Animaux et d'Introduction à l'Anatomie Compare* (Deterville, 1829).
4. Bianchi, D. & Mislan, K. A. S. Global patterns of diel vertical migration times and velocities from acoustics data. *Limnol. Oceanogr.* **61**, 353–364 (2016).
5. Røstad, A., Kaartvedt, S. & Aksnes, D. L. Light comfort zones of mesopelagic acoustic scattering layers in two contrasting optical environments. *Deep Sea Res. Part I Oceanogr. Res. Pap.* **113**, 1–6 (2016).
6. Steinberg, D. K., Goldthwait, S. A. & Hansell, D. A. Zooplankton vertical migration and the active transport of dissolved organic and inorganic nitrogen in the Sargasso Sea. *Deep Sea Res. Part I Oceanogr. Res. Pap.* **49**, 1445–1461 (2002).
7. Bianchi, D., Stock, C., Galbraith, E. D. & Sarmiento, J. L. Diel vertical migration: ecological controls and impacts on the biological pump in a one-dimensional ocean model. *Glob. Biogeochem. Cycles* **27**, 478–491 (2013).
8. Steinberg, D. K. & Landry, M. R. Zooplankton and the ocean carbon cycle. *Ann. Rev. Mar. Sci.* **9**, 413–444 (2017).
9. Churnside, J. H., Wilson, J. J. & Tatarskii, V. V. Lidar profiles of fish schools. *Appl. Opt.* **36**, 6011–6020 (1997).
10. Churnside, J. H. & Thorne, R. E. Comparison of airborne lidar measurements with 420 kHz echo-sounder measurements of zooplankton. *Appl. Opt.* **44**, 5504–5511 (2005).
11. Hostetler, C. A., Behrenfeld, M. J., Hu, Y., Hair, J. W. & Schulien, J. A. Spaceborne lidar in the study of marine systems. *Ann. Rev. Mar. Sci.* **10**, 121–147 (2018).
12. Burt, W. J. & Tortell, P. D. Observations of zooplankton diel vertical migration from high-resolution surface ocean optical measurements. *Geophys. Res. Lett.* **45**, 396–13,404 (2018).
13. Briggs, N. T., Slade, W. H., Boss, E. & Perry, M. J. Method for estimating mean particle size from high-frequency fluctuations in beam attenuation or scattering measurements. *Appl. Opt.* **52**, 6710–6725 (2013).
14. Behrenfeld, M. J. et al. Space-based lidar measurements of global ocean carbon stocks. *Geophys. Res. Lett.* **40**, 4355–4360 (2013).
15. Behrenfeld, M. J. et al. Annual boom–bust cycles of polar phytoplankton biomass revealed by space-based lidar. *Nat. Geosci.* **10**, 118–122 (2017).
16. Stramski, D., Shalapyonok, A. & Reynolds, R. A. Optical characterization of the oceanic unicellular cyanobacterium *Synechococcus* grown under a day–night cycle in natural irradiance. *J. Geophys. Res. Oceans* **100**, 13295–13307 (1995).
17. DuRand, M. D., Green, R. E., Sosik, H. M. & Olson, R. J. Diel variations in optical properties of *Micromonas pusilla* (Prasinophyceae). *J. Phycol.* **38**, 1132–1142 (2002).
18. Dall'Olmo, G. et al. Inferring phytoplankton carbon and eco-physiological rates from diel cycles of spectral particulate beam-attenuation coefficient. *Biogeosciences* **8**, 3423–3439 (2011).
19. Kheireddine, M. & Antoine, D. Diel variability of the beam attenuation and backscattering coefficients in the northwestern Mediterranean Sea (BOUSSOLE site). *J. Geophys. Res. Oceans* **119**, 5465–5482 (2014).
20. Ohman, M. D., Frost, B. W. & Cohen, E. B. Reverse diel vertical migration: an escape from invertebrate predators. *Science* **220**, 1404–1407 (1983).
21. Hannides, C. C. S. et al. Export stoichiometry and migrant-mediated flux of phosphorus in the North Pacific Subtropical Gyre. *Deep Sea Res. Part I Oceanogr. Res. Pap.* **56**, 73–88 (2009).
22. Steinberg, D. K., Lomas, M. W. & Cope, J. S. Long-term increase in mesozooplankton biomass in the Sargasso Sea: linkage to climate and implications for food web dynamics and biogeochemical cycling. *Glob. Biogeochem. Cycles* **26**, GB1004 (2012).
23. Richardson, A. J. In hot water: zooplankton and climate change. *ICES J. Mar. Sci.* **65**, 279–295 (2008).
24. Beaugrand, G., Reid, P. C., Ibañez, F., Lindley, J. A. & Edwards, M. Reorganization of North Atlantic marine copepod biodiversity and climate. *Science* **296**, 1692–1694 (2002).
25. Piontkovski, S. A. & Castellani, C. Long-term declining trend of zooplankton biomass in the Tropical Atlantic. *Hydrobiologia* **632**, 365–370 (2009).
26. Peterson, W. T. & Schwing, F. B. A new climate regime in northeast Pacific ecosystems. *Geophys. Res. Lett.* **30**, 1896 (2003).
27. Chiba, S., Tadokoro, K., Sugisaki, H. & Saino, T. Effects of decadal climate change on zooplankton over the last 50 years in the western subarctic North Pacific. *Glob. Change Biol.* **12**, 907–920 (2006).
28. Archibald, K., Siegel, D. A. & Doney, S. C. Modeling the impact of zooplankton diel vertical migration on the carbon export flux of the biological pump. *Glob. Biogeochem. Cycles* **33**, 181–199 (2019).
29. Behrenfeld, M. J., Boss, E., Siegel, D. A. & Shea, D. M. Carbon-based ocean productivity and phytoplankton physiology from space. *Glob. Biogeochem. Cycles* **19**, GB1006 (2005).
30. Siegel, D. A. et al. Regional to global assessments of phytoplankton dynamics from the SeaWiFS mission. *Remote Sens. Environ.* **135**, 77–91 (2013).

Methods

Field data

Data shown in Fig. 1a provide five examples from the subarctic Pacific in which DVM animals significantly increased ship-measured bbp at night. Data are from a previous study[12], which also provides a full description of the study region, measurement system, data processing and uncertainty analyses. The phytoplankton diel cycle in bbp shown in Fig. 1b was calculated from previously published data[19] and is normalized to 1 at the night-time minimum (Supplementary Discussion).

CALIOP data

CALIOP is the primary instrument on the cloud-aerosol lidar and infrared pathfinder satellite observation (CALIPSO) platform[31], which was launched in 2006. CALIOP measures the total time-dependent return of a pulsed laser output at 1,064 nm and both the co-polarized and cross-polarized return of a 532-nm laser output. The current study is based on night and day differences in the cross-polarized return at 532 nm. The bbp values (available at http://www.science.oregonstate.edu/ocean.productivity/) were calculated from this signal following a previously published study[15], except that bbp at 532 nm was not converted to bbp at 440 nm as in the previous study. In the previous study[15], 30° off-nadir CALIOP tilting manoeuvres were conducted every 2 weeks between 2015 and 2016 to collect ocean measurements with minimal surface backscatter from a wide range of ocean environments. Removing molecular backscatter from the CALIOP parallel channel and combining with data from the cross-polarized channel, we then derived particulate backscatter depolarization ratios and compared these data to collocated MODIS diffuse attenuation (K_d) values. This analysis yielded a linear relationship between CALIOP depolarization ratios and the K_d that was used in the previous study[15] to directly retrieve bbp values from CALIOP without reliance on collocated MODIS observations. This same approach was used for the current study. However, we also further evaluated the relationship between particulate depolarization ratios and K_d at 532 nm using an extensive open-ocean airborne lidar dataset compiled from the 2012 Azores campaign[14], the Ship-Aircraft Bio-Optical Research (SABOR) campaign and three campaigns of the North Atlantic Aerosol and Marine Ecosystem Study (NAAMES)[32] (no airborne data were collected during the fourth NAAMES campaign as mechanical issues grounded the plane). This airborne-based analysis confirmed the previous CALIOP–MODIS finding of a linear relationship between depolarization ratios and K_d, with a mean depolarization:K_d ratio of 1.76 m and s.d. of 0.19 m. Finally, we calculated bbp using a volume scattering function (VSF) at 180° following a previously published study[33] that was developed using measurements from collocated CALIPSO and MODIS 531-nm data. This VSF is consistent with scattering properties for particles in the phytoplankton size domain and it was applied to both day and night CALIOP data. Organisms larger than phytoplankton, such as DVM animals, will have a VSF with a lower efficiency in the backward direction and enhanced efficiency in the forward direction. This difference is one factor (Supplementary Discussion) that influences the relationship between the CALIOP-retrieved DVM backscatter signal and the biomass of these animals, but it is encompassed in the field-based scaling factor between CALIOP $bbp^{night} - bbp^{day}$ data and zooplankton dry weight (see below).

CALIOP merges low-gain and high-gain data onboard to reduce data downlink. The onboard gain ratio calculations fail when there are not enough data for both the low- and high-gain channels, which can happen for night-time cross-polarization measurements. At the beginning of the CALIPSO mission, there was an error in the default values of the gain ratios when the onboard calculation fails. This issue rendered the night-time cross-polarization measurements unusable for ocean bbp retrievals until the error was corrected in late 2007, which is why the current study on night–day differences in bbp was limited to the period of 2008–2017. In addition, advanced microwave scanning radiometer data were used to flag and omit CALIOP retrievals made at wind speeds of ≥9 m s^{-1} to avoid bubble contamination of the bbp values. At wind speeds of <9 m s^{-1}, we also applied a depolarization ratio threshold to remove bubble-contaminated data based on statistical analysis from high-wind conditions.

Calculation of DVM_{CALIOP}

The biomass of DVM animals (DVM_{CALIOP}) was estimated from CALIOP-measured night–day differences in bbp, an estimate of the day-to-night change in bbp due to the phytoplankton diel cycle alone (Fig. 1b), and a scaling factor between backscattering and zooplankton dry weight.

The value of bbp^{night} can be expanded into backscatter by DVM animals (bbp^{DVM}) and backscatter by phytoplankton and other non-migrating particles (bbp^{other}):

$$bbp^{night} = bbp^{DVM} + bbp^{other} \quad (4)$$

The value of bbp^{other} is equal to bbp^{day} corrected for the phytoplankton-based change (c) in bbp from day to night. Rearranging equation (4) and solving for bbp^{DVM} yields:

$$bbp^{DVM} = bbp^{night} - c\,bbp^{day} \quad (5)$$

A variety of factors may influence the value of c, including the daily division rate of the phytoplankton population, the degree to which this division is synchronized around the day–night cycle, the composition of the phytoplankton community[34] and day length. Over much of the PSO, phytoplankton populations are dominated by *Prochlorococcus*, *Synechococcus* and picoeukaryotics species, all of which generally synchronize cell division to the first half of the night[35–39]. We therefore focused on describing c as a function of both division rate (μ; divisions per day) and day length.

First, the dependence of c on μ was determined from a previously published laboratory study[34] and is described by (Extended Data Fig. 5a and Supplementary Discussion):

$$c_1 = 0.929 - 0.122\mu \quad (6)$$

in which the term −0.122 has units of days per division. Equation (6) was applied to MODIS passive ocean-colour-based estimates of μ calculated for the 2008–2017 period (see below). Second, the dependence of c on day length exists because a change in day length causes the two CALIOP sampling points (determined by its fixed orbit) to line up differently with the phytoplankton diel cycle. For the range of day lengths encountered across the PSO, this day length (dl) dependence is described by (Extended Data Fig. 5b and Supplementary Discussion):

$$c_2 = 0.986 + 0.0012\mathrm{dl} \quad (7)$$

in which dl (h) is known precisely for each CALIOP pixel based on date and latitude and the term 0.0012 has units of h^{-1}.

Monthly DVM zooplankton dry-weight data are available at the BATS site over the 2008–2017 CALIOP period. Comparison of these field data to monthly bbp^{DVM} values calculated from equations (5)–(7) for the 2° × 2° CALIOP bin centred on the BATS site yields a mean scaling factor between bbp^{DVM} and DVM biomass of 1,596 g m^{-1} (Supplementary Discussion). Applying this conversion factor gives the following expression for DVM_{CALIOP}:

$$DVM_{CALIOP} = 1,596\left(bbp^{night} - c_1c_2bbp^{day}\right) \quad (8)$$

In Fig. 3c, d, we compare HOT and BATS DVM zooplankton dry-weight data to the CALIOP-retrieved property, Δbbp, simply to maintain consistency with Fig. 3b (Supplementary Discussion). However, DVM biomass should be quantitatively related to the simple difference,

$bbp^{night} - bbp^{day}$. The reason that the seasonal cycle in Δbbp corresponds to that of DVM biomass at HOT and BATS is because bbp^{day} varies little over the year at these two sites, making Δbbp highly correlated ($r^2 > 0.99$, $P < 0.001$) with the simple difference, $bbp^{night} - bbp^{day}$.

Field ADCP data

Global ADCP data were obtained from the Joint Archive for Shipboard ADCP (JASADCP, http://ilikai.soest.hawaii.edu/sadcp/). We selected acoustic backscatter data for the upper 20 m of the ocean surface (equivalent to the sampling depth of CALIOP) from ADCPs with frequencies of 150 or 300 kHz and excluded data from frequencies of 38 and 75 kHz. The frequencies of 150 and 300 kHz better isolate scattering from the small (about 0.5–5 mm) animals that are most likely to be detected by CALIOP owing to their much greater abundances. Backscatter amplitude (E) measurements were converted into acoustic intensity (I_{dB}) following a previously published method[40]:

$$I_{dB} = 10 \log(10^{k_c E/10} - 10^{k_c E_{noise}/10}) \quad (9)$$

in which k_c is a scaling factor used to convert backscatter amplitude counts to decibels (dB) and E_{noise} is the noise floor of the individual ADCP dataset. Values of k_c are frequency-dependent and were taken from a previous study[40]. The noise floor was defined as the minimum $k_c E$ for each individual data file. A total of 7,622 individual paired diel cycles were extracted from the global database (Extended Data Fig. 4). The geographical distribution of these diel cycle data is largely biased to the regions surrounding the Hawaiian Islands, along the Tropical Ocean atmosphere (TAO/TRITON) mooring array in the equatorial Pacific, the Southern California Bight, between Chile and Antarctica, and off the northeast United States seaboard (Extended Data Fig. 4). Detailed inspection of echograms computed from each individual data file revealed occasional time-synchronicity issues, with the apparent deep DVM occurring more than 2 h before or after local sunrise or sunset. To validate the time stamp of each data file, we compared the timing of the mesopelagic (maximum depth of the data file to 150 m) DVM to the time of local sunrise and sunset. Time-synchronicity issues were detected in less than 10% of the data files. The time stamp of these errant ADCP backscattering observations were corrected to synchronize the deep DVM with sunrise or sunset before computing the day–night differences analysed in the manuscript.

Field time-series zooplankton biomass data

Monthly climatological migratory zooplankton dry-weight data shown in Fig. 3c for HOT were calculated using data from Fig. 1 of a previously published study[21]. Monthly climatological migratory zooplankton dry-weight data shown in Fig. 3d for BATS were calculated from data from 1994 to 2017 provided by D.K.S. The 1994–2011 subset of these data has previously been published[22].

Global phytoplankton NPP, biomass, and division rate data

Phytoplankton NPP values used for Fig. 4b, c, phytoplankton division rates (μ) used for calculating c_1 in equation (6) and phytoplankton biomass (C_{phyto}) shown in Extended Data Fig. 6 are from the CbPM[41] using MODIS passive ocean-colour data collected between 2008 and 2017 (data are available at http://www.science.oregonstate.edu/ocean.productivity/).

Reporting summary

Further information on research design is available in the Nature Research Reporting Summary linked to this paper.

Data availability

The CALIOP lidar and field ADCP datasets analysed during the current study are available at http://www.science.oregonstate.edu/ocean.productivity/ and from the Joint Archive for Shipboard ADCP at http://ilikai.soest.hawaii.edu/sadcp/. Source Data for Figs. 3b–d, 4b and Extended Data Figs. 3, 6–8 are provided with the paper.

31. Winker, D. M. et al. Overview of the CALIPSO mission and CALIOP data processing algorithms. *J. Atmos. Ocean. Technol.* **26**, 2310–2323 (2009).
32. Behrenfeld, M. J. et al. The North Atlantic Aerosol and Marine Ecosystem Study (NAAMES): science motive and mission overview. *Front. Mar. Sci.* **6**, 122 (2019).
33. Lu, X. et al. Retrieval of ocean subsurface particulate backscattering coefficient from space-borne CALIOP lidar measurements. *Opt. Express* **24**, 29001–29008 (2016).
34. DuRand, M. D. & Olson, R. J. Diel patterns in optical properties of the chlorophyte *Nannochloris* sp.: relating individual-cell to bulk measurements. *Limnol. Oceanogr.* **43**, 1107–1118 (1998).
35. Vaulot, D., Marie, D., Olson, R. J. & Chisholm, S. W. Growth of *Prochlorococcus*, a photosynthetic prokaryote, in the equatorial Pacific *Ocean. Science* **268**, 1480–1482 (1995).
36. André, J. M., Navarette, C., Blanchot, J. & Radenac, M. H. Picophytoplankton dynamics in the equatorial Pacific: growth and grazing rates from cytometric counts. *J. Geophys. Res.* **104**, 3369–3380 (1999).
37. Vaulot, D. & Marie, D. Diel variability of photosynthetic picoplankton in the equatorial Pacific. *J. Geophys. Res. Oceans* **104**, 3297–3310 (1999).
38. Binder, B. J. & DuRand, M. D. Diel cycles in surface waters of the equatorial Pacific. *Deep Sea Res. Part II Top. Stud. Oceanogr.* **49**, 2601–2617 (2002).
39. Jacquet, S., Prieur, L., Avois-Jacquet, C., Lennon, J. F. & Vaulot, D. Short-timescale variability of picophytoplankton abundance and cellular parameters in surface waters of the Alboran Sea (western Mediterranean). *J. Plankton Res.* **24**, 635–651 (2002).
40. Gostiaux, L. & van Haren, H. Extracting meaningful information from uncalibrated backscattered echo intensity data. *J. Atmos. Ocean. Technol.* **27**, 943–949 (2010).
41. Westberry, T. K., Behrenfeld, M. J., Siegel, D. A. & Boss, E. Carbon-based primary productivity modeling with vertically resolved photoacclimation. *Glob. Biogeochem. Cycles* **22**, GB2024 (2008).

Acknowledgements This work was supported by the National Aeronautics and Space Administration's North Atlantic Aerosol and Marine Ecosystems Study (NAAMES) and EXport Processes in the Ocean from RemoTe Sensing (EXPORTS) study. A.D.P. was supported by the Applied Physics Laboratory Science and Engineering Enrichment Development (SEED) fellowship. This project received funding from the European Union's Horizon 2020 research and innovation program under Marie Sklodowska-Curie grant agreement number 749591.

Author contributions M.J.B. designed the study. M.J.B., P.G., A.D.P., W.J.B., Y.H. and R.T.O. processed data and analysed results. M.J.B., P.G., A.D.P. and R.T.O. prepared display items. M.J.B. wrote the manuscript with contributions from all authors.

Competing interests The authors declare no competing interests.

Additional information
Supplementary information is available for this paper at https://doi.org/10.1038/s41586-019-1796-9.
Correspondence and requests for materials should be addressed to M.J.B.
Peer review information *Nature* thanks Daniele Bianchi and the other, anonymous, reviewer(s) for their contribution to the peer review of this work.
Reprints and permissions information is available at http://www.nature.com/reprints.

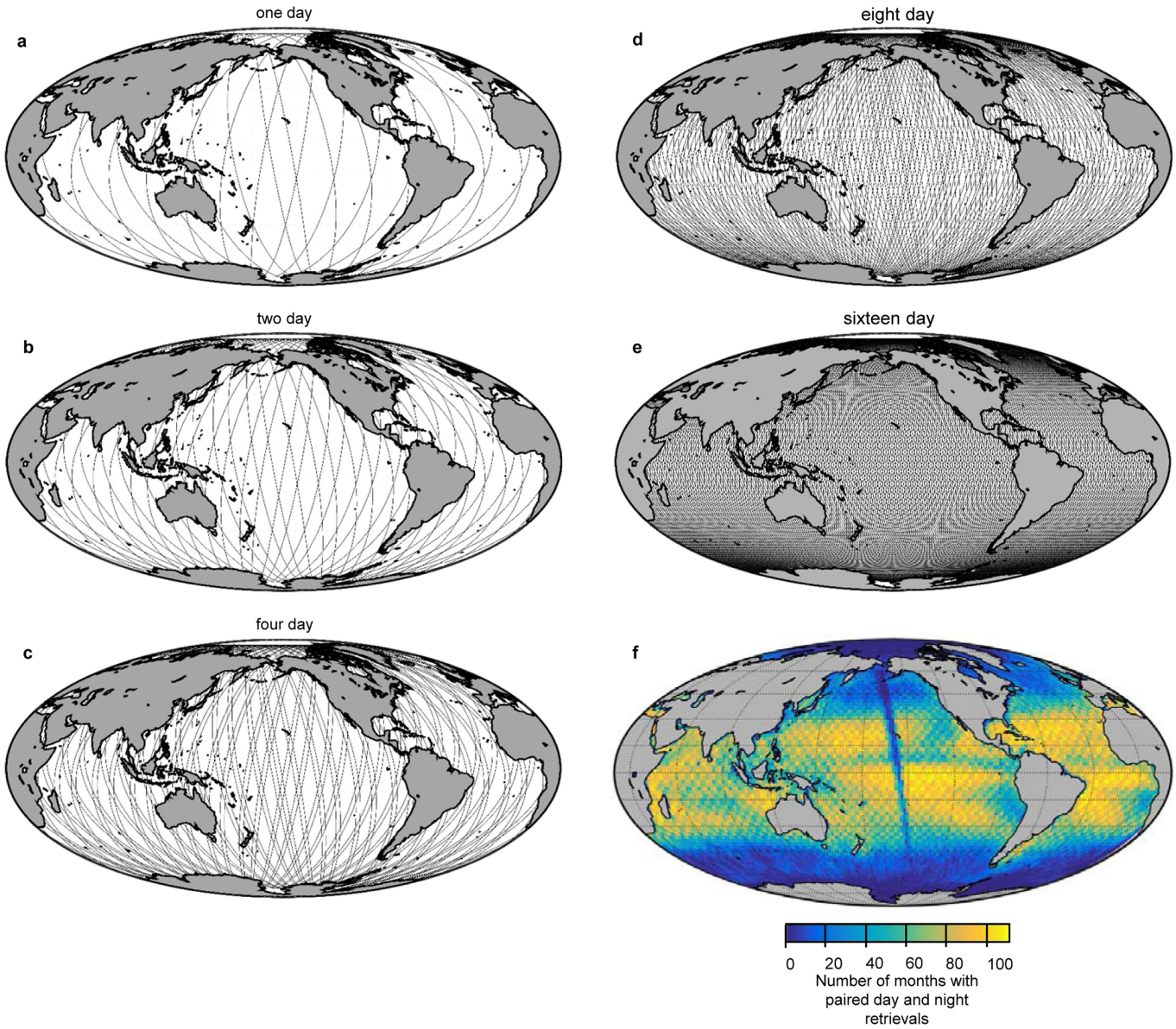

Extended Data Fig. 1 | Global CALIOP observational coverage. a–**e**, CALIOP ground tracks for 1 (**a**), 2 (**b**), 4 (**c**), 8 (**d**) and 16 (**e**) days. **f**, Number of months for each 2° × 2° bin with day and night retrievals of bbp for the 2008–2017 study period. The total number of months possible is 115. The north–south strip of low retrieval success in the middle of the Pacific is caused by a gap in ancillary AMSER surface wind data. AMSER wind data are used for flagging CALIOP data with potential bubble contamination (Methods).

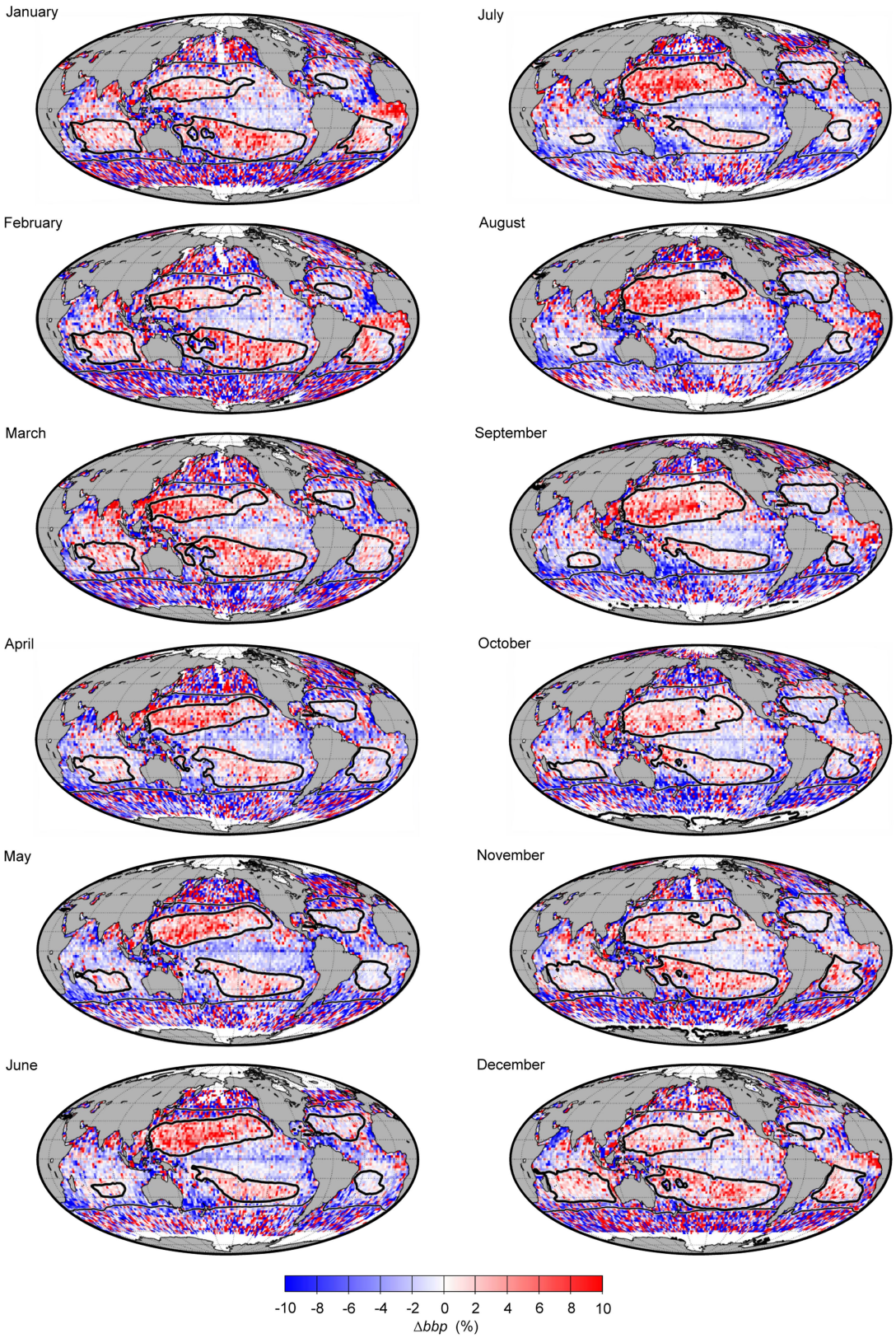

Extended Data Fig. 2 | Global distributions of monthly climatological mean values of Δbbp. Thin black line, contour of monthly mean sea surface temperature of 15 °C. Thick black lines, monthly extent of the 5 subtropical gyres in which annual mean surface chlorophyll concentrations are ≤0.08 mg m^{-3}.

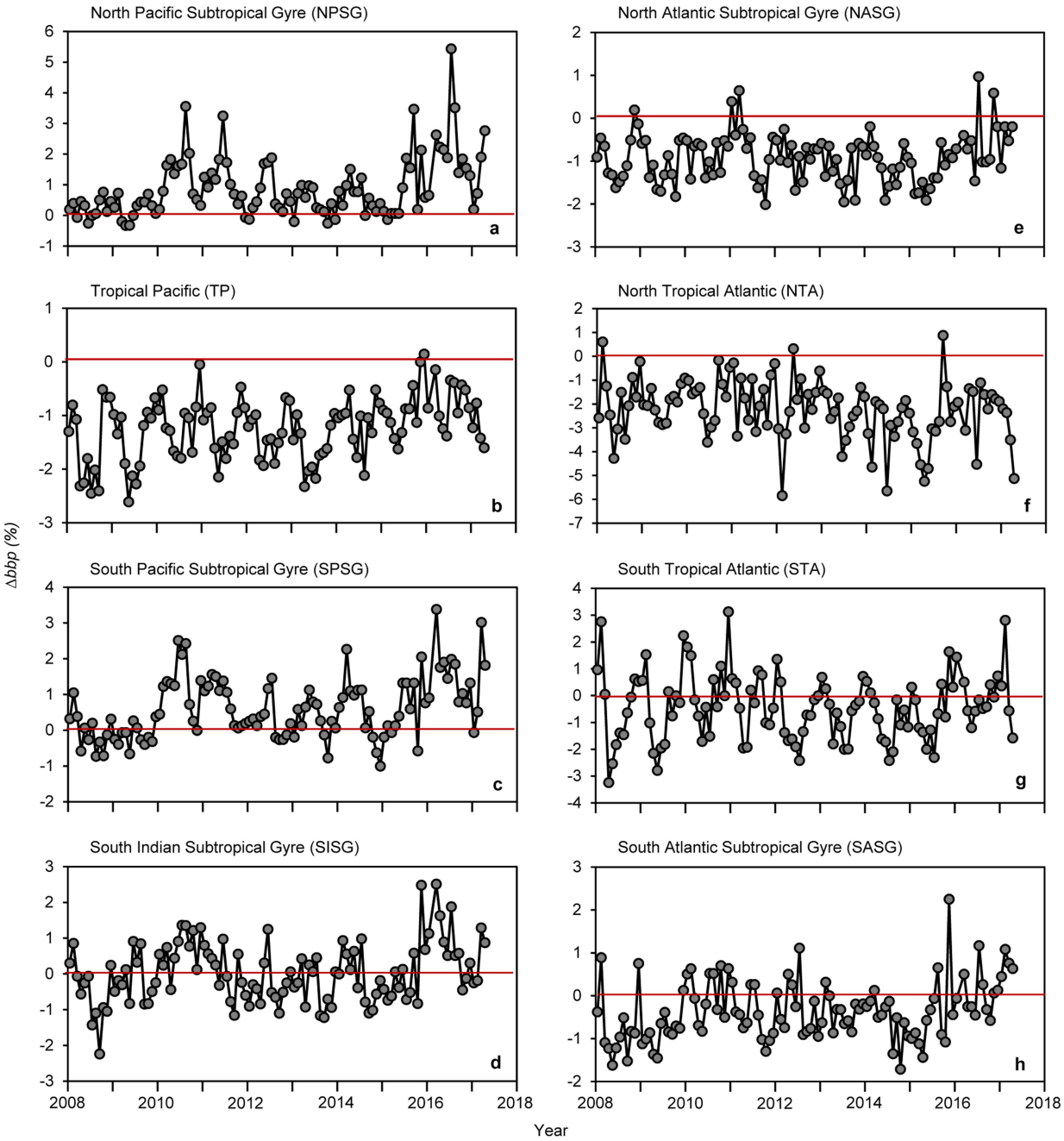

Extended Data Fig. 3 | Time series of Δbbp for the PSO. a–h, The 2008–2017 monthly values of Δbbp (%) for the eight PSO regions described in Fig. 3a.

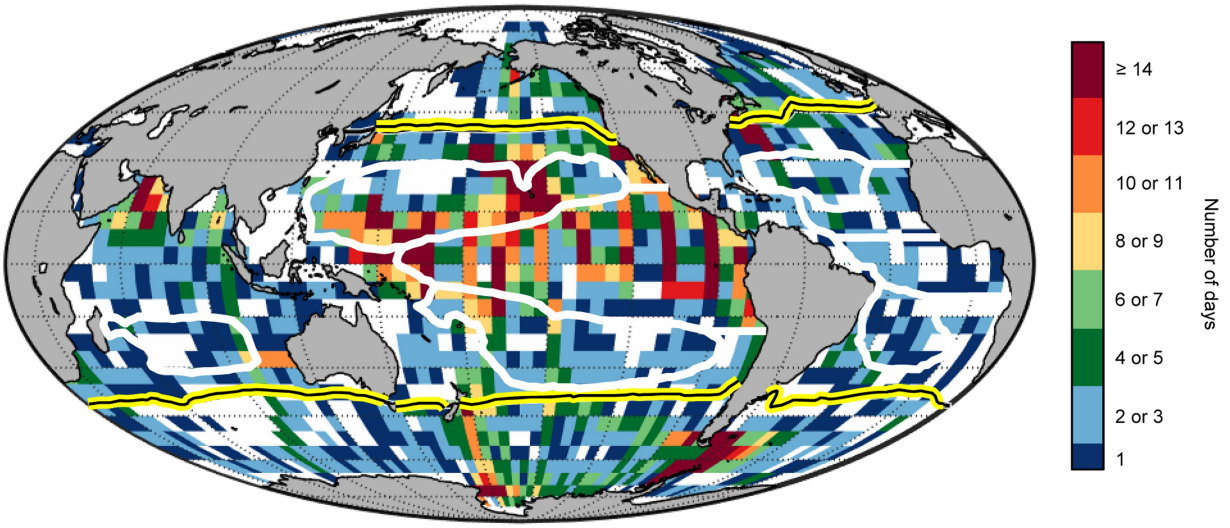

Extended Data Fig. 4 | Global coverage of field ADCP data. Number of days within each 5° × 5° bin for which paired day–night ADCP data are available from the 1985–2017 JASADCP-based field archive (http://ilikai.soest.hawaii.edu/sadcp/). The total number of days possible is 11,680. White bins, no data. Yellow/black line, contour of annual mean sea surface temperature of 15 °C. Thick white lines, boundaries of the eight PSO regions described in Fig. 3a.

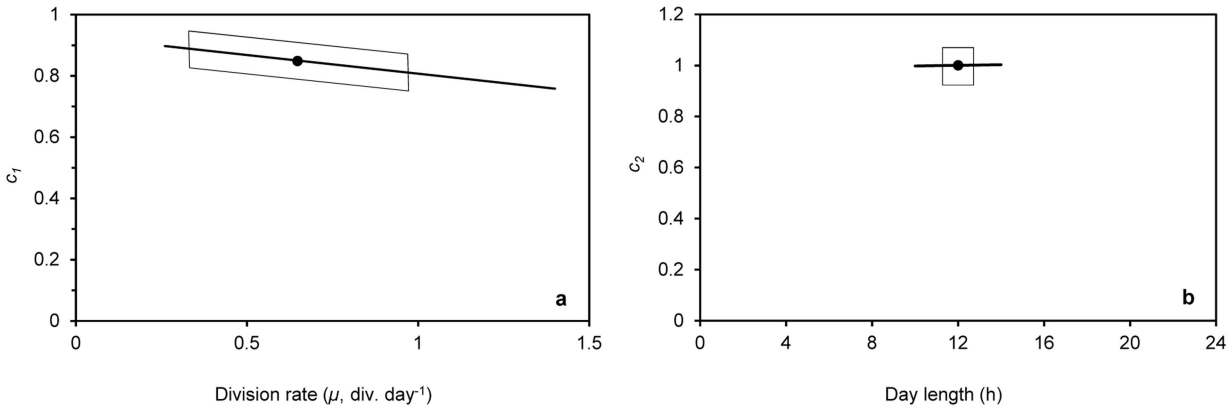

Extended Data Fig. 5 | Influence of phytoplankton division rate and of day length on calculated DVM backscatter for the PSO. a, Values for c_1 (equation (6)) over the range of phytoplankton division rates (μ) in the PSO (n = 999 monthly μ values for all PSO regions). Solid circle, mean value of μ and c_1 for the PSO. The box shows ±1 s.d. of the mean of μ and the solid line shows values of c_1 over the full range in μ for the PSO. **b**, Values for c_2 (equation (7)) over the range of day lengths in the PSO (n = 999 monthly day length values for all PSO regions). Solid circle, mean day length and c_2 value for the PSO. The box shows ±1 s.d. of the mean day length and the solid line shows values of c_2 over the full range in day length for the PSO.

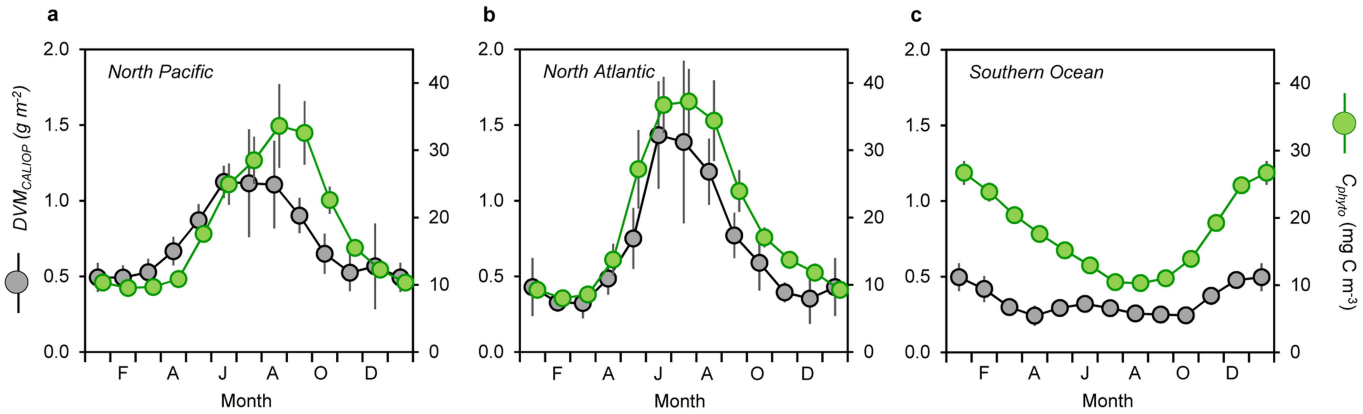

Extended Data Fig. 6 | Seasonal cycles in monthly mean regionally integrated values of DVM_{CALIOP} and phytoplankton biomass for high-latitude regions. a, North Pacific. **b**, North Atlantic. **c**, Southern Ocean. These three regions are described in Fig. 4c. Vertical lines show ±1 s.d. (n = 111 monthly DVM_{CALIOP} (g m^{-2}) and C_{phyto} (mg C m^{-3}) values for each region). C_{phyto} data are from the carbon-based production model (CbPM) and MODIS passive ocean-colour data (Methods).

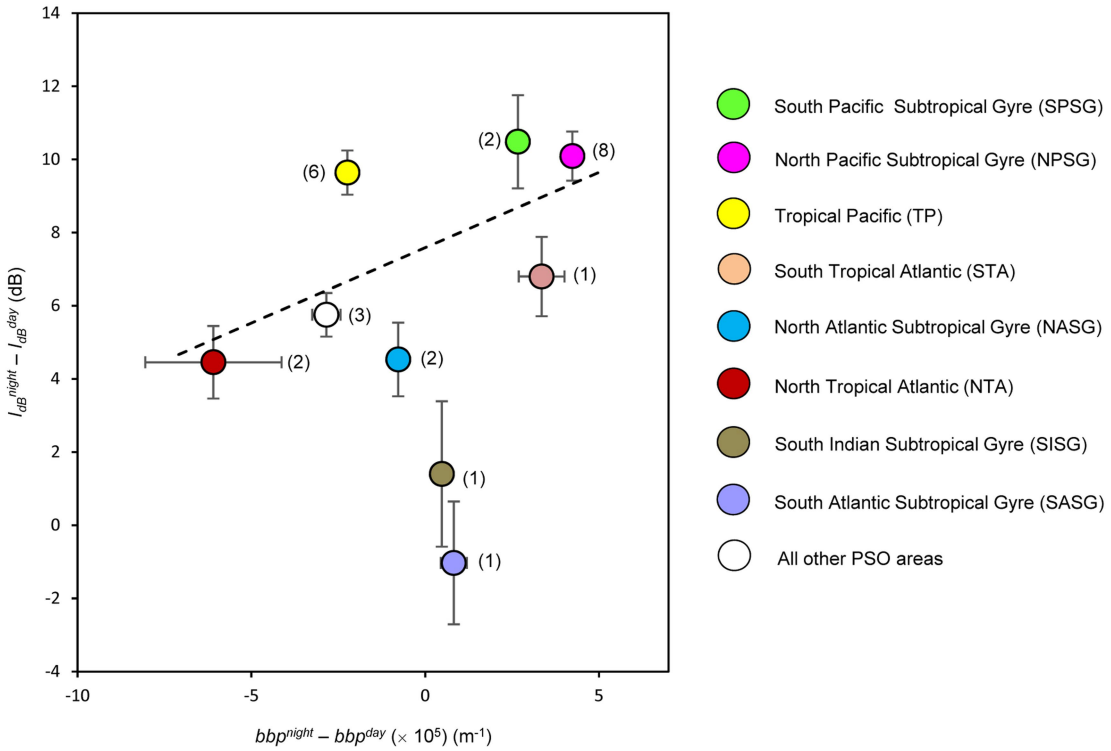

Extended Data Fig. 7 | Comparison of CALIOP night–day bbp differences and field ADCP night–day differences in acoustic backscatter. Dashed line, two-sided least-squares linear regression fit to data for the SPSG, NPSG, TP, STA, NASG and NTA ($n = 6$). For completeness, the mean value for PSO bins outside our eight primary regions is indicated by the white symbol. Symbols, regional mean ±s.e.m. (SISG, $n = 19$; SASG, $n = 18$; TP, $n = 115$; NASG, $n = 16$; NTA, $n = 23$; NPSG, $n = 59$; STA, $n = 22$; SPSG, $n = 59$; other, $n = 302$). Symbol colours identify region (labelled on the right) and correspond to the colours shown in Fig. 3a. Numbers next to each symbol indicate the median number of days with ADCP data within the 32-year field record for the 5°× 5° bins.

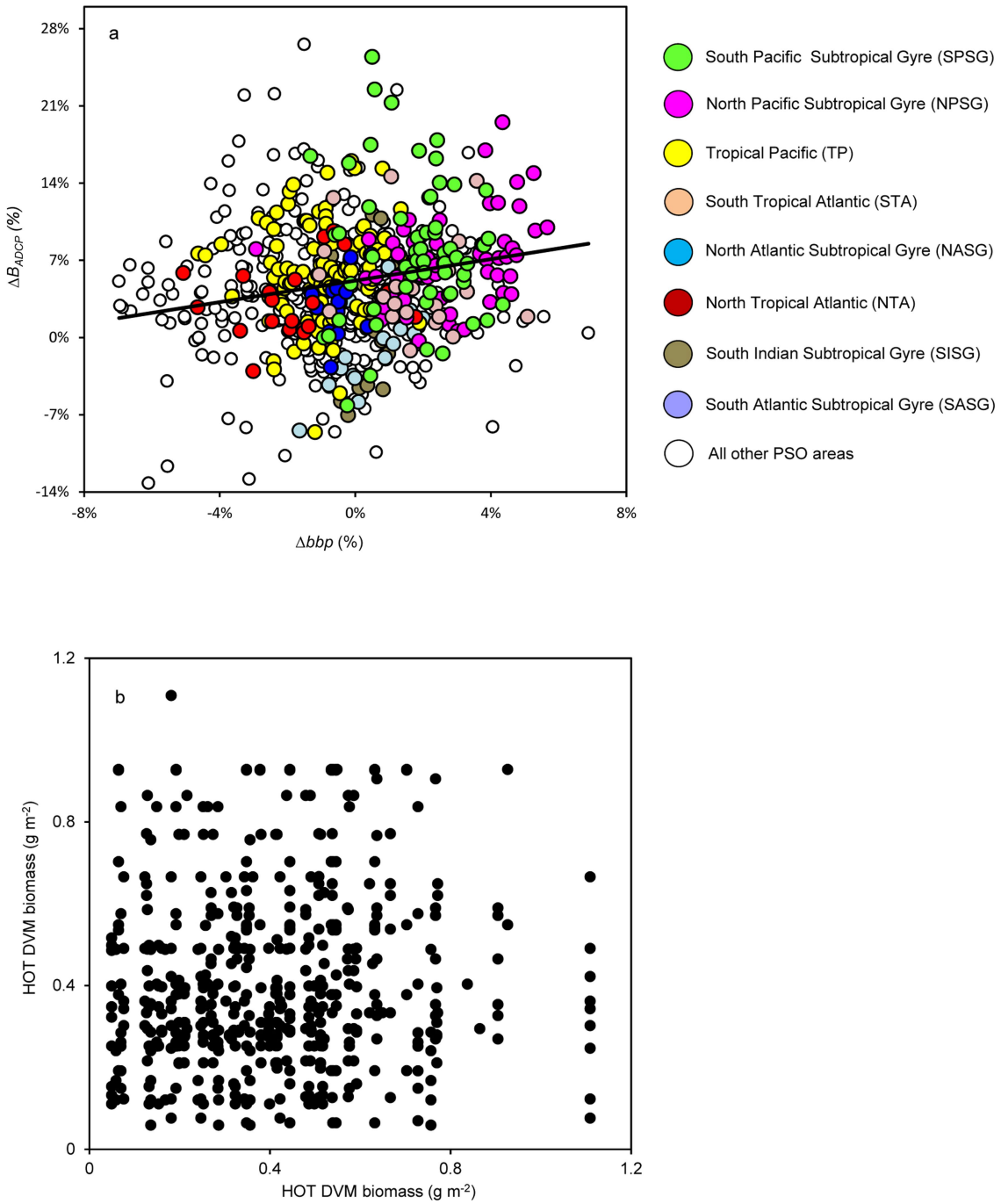

Extended Data Fig. 8 | Bin-to-bin comparison of CALIOP Δbbp and field-based DVM measurements in the PSO. a, CALIOP normalized difference ratios (Δbbp) versus field ADCP (ΔB_{ADCP}) normalized difference ratios for 5° × 5° bins within the PSO. Black line, two-sided least-squares linear regression fit (*F*–test *P* value for slope; $P < 0.001$; $n = 331$ independent geographical bins) for all data from our eight primary PSO regions (coloured symbols are labelled on the right). White symbols, PSO values for 5° × 5° bins outside of the 8 primary regions. Inclusion of these data in the linear regression analysis increases the *F*-test value to $P = 0.005$ ($n = 633$ independent geographical bins). **b**, Relationship between field DVM biomass at the HOT site measured for a given calendar month and year (*x* axis) versus DVM biomass measured during all other years for the same calendar month (*y* axis).

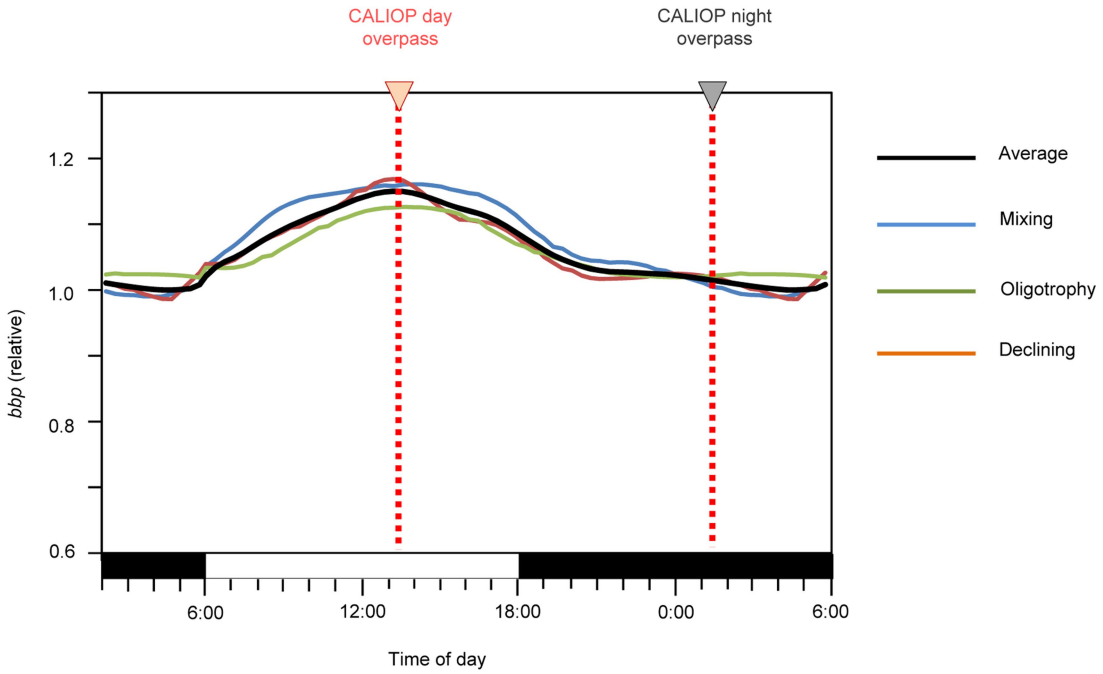

Extended Data Fig. 9 | Field-based diel cycles in bbp. Mean diel cycles in bbp from a previous study[19] for mixing (blue line; $n = 69$ days of measurements), oligotrophy (green line; $n = 322$ days of measurements) and declining (red line; $n = 32$ days of measurements) conditions and the mean of these three cycles (black line), which corresponds to the diel cycle in Fig. 1b.

Supplementary Discussion

This file includes supplemental text for the manuscript, “Satellite-observed daily vertical migrations of global ocean animals”, by Behrenfeld *et al*. regarding (1) CALIOP orbits and data binning, (2) high-latitude spatial variability in CALIOP retrievals, (3) normalized difference ratio data and results in figure 3 of the main manuscript, (4) calculation of the phytoplankton diel *bbp* cycle, (5) additional details on calculations of DVM biomass, and (6) directions for future research.

1) CALIOP orbits and data binning: While satellite lidar measurements have become a common tool for atmospheric research, they are relatively new for studying ocean ecosystems[11,14,15]. Unlike familiar passive ocean color instruments that use a rotating telescope or ‘push-broom’ approach to achieve broad-swath measurements, the CALIOP instrument conducts its measurements at a near-nadir angle and only along its orbit tracks, which are oriented along the ground in opposite directions on the daylight and dark sides of the Earth. Extended Data Figure 1a shows day and night orbits for a single 24 hour period, illustrating how rare orbit cross-over points are for collecting spatially coincident data within a single day (and ocean retrievals for many of these will be prevented by clouds). Furthermore, even when ocean retrievals are successful at both times for a given cross-over point, the water sampled during the day will be different than that measured 12 hours later at night because surface waters are continuously moved by ocean currents. Because of these considerations, we used binned CALIOP data to evaluate global patterns in DVM animals rather than focusing only on spatially coincident data. Binning was also necessary for comparing CALIOP results to field data (which are also spatially and temporally sparse).

While not providing broad swaths of data like an ocean color sensor, advantages of CALIOP are that it provides measurements during the day and night and its rapid laser pulse rate enables measurements every 330 m along the ground. In addition, its precessing orbit allows for fully-global sampling over its 16-day repeat cycle. Extended Data Figures 1a-e illustrate how this global coverage builds-up over 1, 2, 4, 8, and 16 days. Thus, for a given spatial binning resolution, the CALIOP approach can provide a dense within-bin 'sampling' over the course of a month. Averaging these repeated measurements within a monthly bin reduces noise in the retrieved ocean property and allows the signal of interest to be isolated. As discussed in **Section 2** below, the number of successful day and night retrievals within a bin depends on atmospheric conditions (cloud cover, aerosol thickness), which vary strongly with latitude.

In our first publication using CALIOP data[14], we validated satellite-retrieved *bbp* values using coincident ship-based and airborne-based field measurements. We then binned global CALIOP data into 2^o latitude $\times$ 2^o longitude bins to evaluated global patterns in phytoplankton biomass and total particulate carbon concentration. The same $2^o \times 2^o$ binning was used in the current manuscript for figure 2. In our second CALIOP publication[15], we demonstrated an excellent agreement between CALIOP and ocean color based seasonal cycles in *bbp* and then used $1^o \times 1^o$ binned data to evaluate phytoplankton bloom dynamics. This slightly higher spatial resolution was used because the study was geographically restricted to the north and south polar regions, whereas $2^o \times 2^o$ binning is appropriate for the global scope of the current study. For figure 3b of the current manuscript, a coarser resolution of $5^o \times 5^o$ was used because of the very sparce coverage of ADCP data. Finally, $6^o \times 6^o$ binning was used for figure 4c because (1) smaller bins

make it difficult to distinguish the outlines and dots used for each bin that indicate statistical significance and (2) the enhanced signal-to-noise of the larger bins improves detection of temporal trends (i.e., de-seasoned anomalies) in DVM_{CALIOP}.

2) High-latitude zones: At latitudes poleward of the PSO, CALIOP retrievals of the DVM signal remain noisy between the spatial bins used for our analysis. In contrast, these retrievals exhibit significantly better spatial coherence within the PSO. Consequently, we have largely restricted our more detailed analyses of the CALIOP record to these lower-latitude PSO regions. A number of factors contribute to the noisy spatial maps of the DVM signal at high latitudes. First and foremost of these factors is the combined impact of spatial and temporal variability in plankton ecosystems, persistent cloudiness, and the sampling coverage of CALIOP. Extended Data Figure 1f shows the total number of months within the 2008 – 2017 period (115 total possible) for each 2^o latitude x 2^o longitude bin with at least one day and one night retrieval of *bbp*. This latter figure clearly shows the much poorer coverage at high latitudes, but even this stark difference between high latitudes and the PSO over-represents high-latitude coverage. CALIOP's small single-shot footprint (100 m at the ocean surface) allows successful retrievals between even small gaps in cloud cover. Thus, even if a given bin is largely overcast for an entire month (as is often the case at higher latitudes), a single day and night retrieval through gaps in the clouds would yield a day-night pair for that month and add to the total number of measurement pairs for that bin in Extended Data Figure 1f. These two points could come from different locations anywhere within the 2^o x 2^o bin and may be separated in time by nearly a month. In such a case, spatial and temporal variations in the plankton community can be a large contributor to the calculated night-day difference. As cloudiness decreases from this extreme

example, many more CALIOP retrievals can be averaged together within a given 2^o x 2^o bin, thereby dampening the influence of plankton community spatial and temporal variations and better isolating the DVM signal (as discussed above). In the PSO, clear sky scenes are far more common than at higher latitudes. With a 100 m single-pulse footprint and a 330 m ground distance separation between pulses, >600 measurements can be collected within a given 2^o x 2^o bin on a single day or night overpass under clear skies. With clear sky conditions for even two overpasses per month, this means that >1200 daytime measurements and >1200 nighttime measurements spanning the breadth of the bin may be available to calculate a single monthly average night-day difference. In addition, temporal variability in plankton stocks within the 2^o x 2^o bins of the PSO tend to be smaller than most high-latitude bins. Thus within the PSO, effective retrieval of the DVM signal at $2^o \times 2^o$ binning resolution is far more likely than at higher latitudes. One solution to the 'spatial speckling' problem at high latitudes is to average data over a much larger area. When we do this, we find that regionally-integrated annual average DVM_{CALIOP} for the three high-latitude regions shows a relationship with annual average mixed layer net primary production that is highly consistent with that found for the PSO regions [Fig. 4b]. Furthermore, regionally-integrated monthly DVM_{CALIOP} data for the three high-latitude regions exhibit strong annual cycles consistent with both the magnitude and seasonality of phytoplankton biomass in these regions [Extended Data Fig. 6].

In addition to the above considerations regarding high latitude retrievals, phytoplankton community composition in these regions tends to be more diverse than in the PSO, division rates vary strongly with season and are poorly constrained by satellite productivity algorithms, and it is highly likely that cell division cycles are often not synchronized to the daily light-dark cycle.

The impact of these ecological considerations on the phytoplankton night-day difference is currently unresolved (see **Section 6** below).

3) Normalized difference ratios: In figure 2 of the main manuscript, we compare CALIOP retrievals of Δbbp with normalized difference ratios calculated from field ADCP measurements. We used normalized difference ratios (equations 1 and 2 in the main manuscript) for this comparison for two primary reasons. First, division of night-day differences by daytime values makes the retrieved property biomass-specific, allowing an evaluation of the relative contribution of DVM animals. Second, normalization to daytime values, at least in part, helps reduce the influence of instrument-dependent variations in the field measurements. Specifically, the ADCP acoustic backscatter record used in the current study was compiled from more than 30 research vessels and 2,000 field surveys. Differences between the instruments used, how they are mounted, and how they are calibrated can generate instrument-dependent differences in the resultant backscattering data that are not linked to real differences in *in situ* particle backscattering. By calculating the normalized difference ratio, the influence of this instrument-dependent contribution is reduced. To illustrate the significance of this normalization, the ADCP-CALIOP comparison presented in figure 3b of the main manuscript was revised by substituting the normalized difference ratios with simple differences (i.e., y-axis = $I_{dB}^{night} - I_{dB}^{day}$; x-axis = $bbp^{night} - bbp^{day}$) for each data set [Extended Data Fig. 7]. The outcome of this analysis is similar to the result presented in figure 3b of the main manuscript. Specifically, (1) the relative location of each regional average value is the same between graphs and (2) results for the SISG and SASG regions deviate from the other regions in the same manner in both graphs. The primary difference (as expected from the above discussion) is that the linear regression on the

regional ADCP and CALIOP values shown in figure 3b gives an $r^2 = 0.55$ and $p = 0.09$, whereas the same comparison for data in Extended Data Fig. 7 gives an $r^2 = 0.39$ and $p > 0.10$.

In figures 3c and 3d, we also compare Δbbp to DVM biomass measured at the HOT and BATS sites. The expectation is that, across the PSO, DVM biomass will be more quantitatively related to the simple difference, $bbp^{DVM} = bbp^{night} - c\ bbp^{day}$, than the normalized difference ratio. Since bbp^{DVM} and Δbbp have nearly the exact same seasonal cycle at HOT and BATS ($r^2 = 0.99$, $p < 0.001$), we chose to show the CALIOP normalized difference ratio data in figures 3c and 3d simply to be consistent with figure 3b. However, as described in the main manuscript, the actual calculation of DVM biomass is based on the simple difference, bbp^{DVM}.

As discussed in the main text and in the Methods section, creating an adequate field data set (with respect to PSO coverage) for comparison with CALIOP data required aggregating historical ADCP data from over 30 years (1985 to 2017). Even over this long period, most of our 5^o x 5^o bins have only one to a few days of data, and many of these observation pre-date CALIOP. Due to this paucity of data and their temporal mismatches with CALIOP, figure 3b in the main manuscript focuses on the correspondence between regional values of ΔB_{ADCP} and Δbbp. However, we also report that linear regression analysis of ΔB_{ADCP} and Δbbp data for all 5^o x 5^o bins within the eight primary PSO regions yielded a highly significant slope similar to the relationship calculated from the regionally binned data. Extended Data Fig. 8a shows this relationship, where data are color-coded following the regional coloring scheme shown in figure 3a of the main manuscript. As expected, the relationship for all individual data exhibits significant scatter around the least squares linear regression line ($r^2 = 0.04$). We can use the

HOT time series field measurement of DVM biomass to put this result in context. Specifically, we can ask how much predictive skill does knowledge of DVM biomass during a given month of a given year provide in estimating DVM biomass for the same month but other years in the HOT record. This result is shown in Extended Data Fig. 8b. The implication here is that there is a large amount of year-to-year variability in monthly DVM biomass within field records and thus considerable scatter is expected between CALIOP and field ADCP data when compared at the level of individual measurements [Extended Data Fig. 8a], particularly when the two data sets are collected during different years. However, when data are averaged over time and space, clear regional differences emerge in DVM strength and these patterns are consistent between the ADCP and CALIOP records for all PSO regions except the SASG and SISG [Fig. 3b] (see **Section 6** below). A corollary to this result is found in the published studies of Hannides et al.[21] and Steinberg et al.[22], where an annual cycle in DVM biomass becomes clear by calculating monthly average values for field records extending a decade or more. Because of the large variability between years in the monthly data [e.g., Extended Data Fig. 8b], these cycles are difficult to decipher in the full time-series records.

4) Phytoplankton diel *bbp* cycle: Historical studies on diel cycles in ocean inherent optical properties have largely focused on the particulate beam attenuation coefficient[42-44]. To our knowledge, the only published account of diel cycles in *bbp* are from Kheireddine and Antoine[19]. In their study, five years of *bbp* data were evaluated from the long-term, deep-water (2440 m) BOUSSOLE buoy site in the Mediterranean Sea. Over this period, 1322 total days of data were collected, from which the authors selected 737 days of highest data quality. These data were then separated into mixing, declining, oligotrophic, and bloom-climax phases with respect to

phytoplankton biomass. A vast majority of the data were from the three former phases, which are most representative of the PSO. The average diel cycle in *bbp* for each of these phases is reproduced as the blue, red, and green lines, respectively, in Extended Data Fig. 9. The average of these three diel cycles is shown as the black line in Extended Data Fig. 9 and this averaged cycle corresponds to the diel cycle shown in figure 1b of our main manuscript. The bloom-climax data in (19) exhibits a similar diel cycle as during the other seasons but with a daytime peak ~2 hour later in the afternoon.

5) DVM biomass calculations: The biomass of DVM animals (DVM_{CALIOP}) was calculated from CALIOP-measured night (bbp^{night}) and day (bbp^{day}) differences in *bbp* following [Eq. 3 of main manuscript]:

$$DVM_{CALIOP} = a\,(bbp^{night} - c_1\,c_2\,bbp^{day}),$$

where c_1 accounts for growth rate (μ; divisions day^{-1}) dependent night-day differences in *bbp* due to the phytoplankton diel cycle [Fig. 1b], c_2 accounts changes in night-day *bbp* differences caused by variations in day length, and a is an empirical conversion factor between the backscatter signal of DVM animals (bbp^{DVM}) and zooplankton biomass. In the following three subsections, we provide details on the derivation of c_1, c_2, and a.

For the current study, we did not attempt to introduce an additional correction factor to account for community composition effects on the phytoplankton diel *bbp* cycle because (1) community composition is relatively conserved in the open ocean regions of the PSO (at least compared to higher latitude and coastal regions), (2) very little is known from targeted field or laboratory studies about taxonomic influences on the diel *bbp* cycle, and (3) satellite-based global

determinations of phytoplankton community composition are still relatively immature and would likely add more errors than improvements in our estimates of DVM_{CALIOP}. Beyond taxonomic considerations, we also evaluate whether regional time series in bbp^{night} - bbp^{day} covaried with other globally-retrieved ocean properties (surface chlorophyll *a* concentration, euphotic zone depth, median mixed layer light level, surface PAR, mixed layer depth, sea surface temperature), but found no unique relationships consistent across regions that could not be attributed to corollary relationships between these other ocean properties and variations in phytoplankton growth rates.

Dependence on division rate: Very few controlled studies have been conducted that enable a quantitative assessment of growth rate dependent variability in the phytoplankton diel *bbp* cycle. One notable exception is the study of DuRand and Olson[34]. In that study, diel cycles in scattering cross section were reported for cultures of *Nannochloris* (chosen as representative of the small phytoplankton found in oligotrophic waters) grown under daily light-dark irradiance cycles of intensity ranging from 60 to 1500 µmole photons m^{-2} s^{-1}. Cell division cycles in all cultures were tightly phased with the light:dark cycle, with division occurring in the dark (as is the case in the PSO). The relationship between growth irradiance and μ (divisions day^{-1}) was extracted from figure 3 of DuRand and Olson[34]. Daytime maxima and nighttime minima in scattering cross section were extracted for each growth condition from figure 6 of DuRand and Olson[34]. The relationship between these minimum and maximum values and values that would be observed during the CALIOP measurement times was calculated using the field-based diel cycle in figure 1b of the current manuscript (see **Section 4** above). A two-sided least squares linear regression analysis was then conducted on the relationship between the night-day

difference in these scattering values and μ ($r^2 = 0.40$, $p = 0.12$, $n = 6$). However, this relationship does not provide a description of c_1 because it is based on a pure phytoplankton culture, whereas *bbp* data from CALIOP includes additional 'background' scattering from other non-phytoplankton components. This issue was addressed by considering the results presented in figure 1b where the field-measured diel cycle in *bbp* gives a day-to-night decrease in *bbp* of ~15%. These field data were collected in the Mediterranean Sea where the dominant prokaryotic and picoeukaryotic phytoplankton divide at a rate slightly less than 1 division day^{-1}. Thus, assuming a bulk phytoplankton division rate of ~0.8 division day^{-1}, a 'background' *bbp* signal was added to our DuRand and Olson[34] based two-sided linear regression result until a value for c_1 of 0.85 was achieved for $\mu = 0.8$ division day^{-1}. This resultant description for c_1 is:

$$c_1 = 0.929 - 0.122\ \mu.$$

The mean, standard deviation, and range for c_1 values in the PSO are shown in Extended Data Fig. 5a.

Dependence on day length: The dependence of *c* on day length exists because a change in day length causes the two CALIOP sampling points (determined by its fixed orbit) to line up differently with the phytoplankton diel cycle. To account for this effect, the field-based diel cycle in *bbp* shown in figure 1b was split into its daytime and nighttime components. The duration of these day and night components was then expanded and contracted to create diel cycles for day lengths ranging from 4 to 20 hours (i.e., outside this range both CALIOP measurement times either occur in the day or the night). The night-day difference in *bbp* was then calculated for the two CALIOP measurement times for each day length. For the highly constrained range in day length across the PSO (10 – 14 h), the relationship between these night-

day difference values and day length is linear ($r^2 = 1.0$, $p < 0.001$). This relationship was then adjusted to give a value of 1 for a 12:12 day:night cycle (i.e., the day length corresponding to the data in figure 1b). The resultant relationship is:

$$c_2 = 0.986 + 0.0012\ dl,$$

where dl = day length (h). The mean, standard deviation, and range for c_2 values in the PSO are shown in Extended Data Fig. 5b, with the full range being highly constrained to $c_2 = 0.998$ to 1.002. Thus, inclusion of c_2 in our calculation of DVM biomass is more for completeness than as an important correction in the calculation of DVM_{CALIOP}.

Over a broader range of day lengths, the relationship between night-day difference values and day length becomes nonlinear and, when normalized to 1 for a 12:12 day:night cycle is described by ($r^2 = 1.0$, $p < 0.001$):

$$c_2 = -7E\text{-}06\ dl^4 + 0.0004\ dl^3 - 0.0069\ dl^2 + 0.06\ dl + 0.8013,$$

which for a day length range of 4 to 20 hours gives a slightly larger range of values for c_2 of 0.952 to 1.006.

Scaling bbp^{DVM} to DVM_{CALIOP}: Our primary motivation for scaling bbp^{DVM} to DVM_{CALIOP} was to convert the former property with units of m^{-1} into a more ecologically-understandable property with units of g m^{-2} dry weight. For this conversion, we use a constant scaling factor, meaning that the results shown in figure 4 of the main manuscript can be interchanged between the directly-measured CALIOP property, bbp^{DVM}, and the scaled biomass property, DVM_{CALIOP}. Our approach for quantifying the scaling factor between bbp^{DVM} to DVM_{CALIOP} was similar to that used for more standard satellite ocean color products, such as surface chlorophyll concentration.

Specifically, we used field data collected coincidently (in this case at the monthly time scale) with CALIOP. For the current study, this means that we limited our analysis to BATS field data collected between 2008 and 2017, which yielded a conversion factor of 1596 g dry weight m^{-1}. If we had instead combined these BATS data with monthly average DVM biomass data from HOT (1994 to 2005) adjusted for the apparent 23% increase since the end of the field record (see main manuscript), then the resultant conversion factor would have been 1402 g dry weight m^{-1}.

6) Future directions: The current manuscript describes the first attempt to connect a satellite-retrieved property (*bbp*) to animal biomass and distributions in the global ocean. As is standard practice in satellite oceanography, we have used the best available *in situ* observations (ADCP and zooplankton biomass time-series data) to validate the CALIOP retrievals before attempting an interpretation of their ecological meaning. As should be expected with any such new satellite product, additional future studies and new technologies are needed to both evaluate and constrain uncertainties in our analysis and to expand upon the capabilities of CALIOP for studying global ocean DVM animals. The following list provides some examples.

i. <u>*Phytoplankton diel bbp cycle*</u>: CALIOP retrieved Δbbp span from negative to positive values because nighttime increases in *bbp* from DVM animals are countered by a background phytoplankton diel cycle that decreases *bbp* from day to night. We have used data from the only published study that has quantified the phytoplankton diel *bbp* cycle in the field[19]. These data were collected at a single location in the Mediterranean Sea and, while a range of phytoplankton populations were encountered during that study, similar analyses are needed in other ocean regions with different phytoplankton

populations to evaluate the robustness of our description of phytoplankton diel *bbp* changes. These analyses should include populations where cell division of the dominant species are synchronized over the diel cycle and also populations where cell division is not synchronized, as the latter case is likely common at higher latitudes.

It is important to recognize that the assessment of phytoplankton diel *bbp* cycles in the field is not as straightforward as it might initially appear. The problem is that the cycle of interest is the biomass-normalized cycle, so an appropriate (preferably independent) assessment of biomass is needed, particularly when measurements are conducted on a moving ship. One potential approach is to divide *bbp* by coincident measurements of chlorophyll concentration, but this approach will typically fail because cellular chlorophyll concentrations also have a diel cycle of their own that will result in an incorrect cycle for biomass-normalized *bbp*. In the study of Kheireddine and Antoine[19], measurements were conducted from a fixed location (rather than a moving ship) and *bbp* values measured over each diel cycle were normalized to the value measured at dawn. However, even for this study, physical advection of the surface layer ensures that different populations were sampled over each diel cycle, which may largely be the reason that this earlier study typically found that *bbp* values at the end of a given diel cycle were not the same as at the beginning[19]. A great advantage of the Kheireddine and Antoine[19] study was that investigators had a large number of daily cycles in *bbp* to work with and thus, through averaging, they arrived at consistent cycles under various growth conditions (see **Section 4** above).

An alternative approach for addressing uncertainties in the phytoplankton diel *bbp* cycle would be to conduct a series of laboratory experiments (much like that of DuRand and Olson[34]) where different phytoplankton species are synchronized to light-dark cycles of various durations and changes in *bbp* are continually monitored over the diel cycle. Such experiments should also encompass a range in growth rates for each species to enable development of predictive relationships.

ii. *DVM biomass*: In the current study, we convert CALIOP retrievals of bbp^{DVM} into an estimate of DVM animal biomass using data from a single field time-series data set (i.e., BATS). This conversion was largely conducted to put CALIOP results in more intuitive ecological units (see **Section 5** above), but there is significant uncertainty in this single conversion factor. Specifically, the backscattering efficiency of DVM animals depends on animal size, shape, composition, and other factors and the CALIOP-coincident BATS time-series data do not encompass every type of DVM animal found in the global oceans. Achieving more accurate estimates of DVM_{CALIOP} from bbp^{DVM} will require a broader diversity of field samples, an increase in the number of time-resolved DVM animal properties characterized, and a detailed optical model linking these properties to backscattering.

iii. *Spatial sampling*: As discussed in detail above, spatial binning is required to achieve low-noise day-night match-up data with CALIOP. These binned data must then be validated with field observations that are typically collected at much smaller scales (e.g., the size of the opening of a zooplankton net or the footprint of a ship ADCP). A future

study is needed to assess uncertainties in this spatial disconnect by providing a direct measurements that span the sampling scales of field zooplankton and CALIOP data. One potential approach here would be to couple ship-based DVM animal and backscattering measurements with airborne lidar measurements. In this scenerio, the airborne measurements could be conducted along a flight pattern that encompasses the retrieval scale of a satellite lidar, and might even be coordinated with simultaneous CALIOP overpasses (as in Behrenfeld et al.[14]), assuming CALIOP is still operational.

iv. *South Indian and South Atlantic Subtropical Gyres*: When regionally-averaged field ADCP and CALIOP data are compared [Fig. 3B, Extended Data Fig. 7], results for the SISG and SASG deviate from the other PSO regions. Potential reasons for this discrepancy are discussed in the main manuscript. Of particular concern is the low number of ADCP data available for these two regions in the historical record and their temporal disconnect with the CALIOP record. However, it is noteworthy that the individual bin data for the SISG and SASG actually span a considerable fraction of the range of variability in Δbbp and ΔB_{ADCP} found for the other PSO regions [Extended Data Fig. 8a]. Clearly, additional field sampling campaigns are needed in the SISG and SASG to investigate the underlying basis of the apparent discrepancy in regionally-averaged Δbbp and ΔB_{ADCP} values.

v. *New technology*: CALIOP was designed for atmospheric science, not ocean applications. It provides information on ocean *bbp* for only a single 22 m depth bin immediately below the ocean's surface. High Spectral Resolution Lidar (HSRL) instruments have been

developed since the launch of CALIOP and extensively field demonstrated from aircraft over a diversity of ocean regimes. These instruments can retrieve *bbp* values deep within the sunlit surface layer of the ocean with meter-scale vertical resolution. If this technology is transferred to a satellite instrument, the HSRL approach could yield both improved accuracy in *bbp* retrievals and an assessment of DVM animal nighttime vertical distributions. It is conceivable that vertically resolved DVM retrievals could provide information on feeding behavior linked to phytoplankton production layers and more accurate assessments of DVM biomass, as only those DVM animals that reach the upper 22 m of the surface are currently detected by CALIOP.

References

42. Siegel, D.A., Dickey, T.D., Washburn, L., Hamilton, M.K., & Mitchell, B.G. Optical determination of particulate abundance and production variations in the oligotrophic ocean, *Deep Sea Res. Part A* **36,** 211–222, doi:10.1016/0198-0149(89)90134-9 (1989).

43. Stramski, D., Shalapyonok, A., & Reynolds, R. A. Optical characterization of the oceanic unicellular cyanobacterium *Synechococcus* grown under a day-night cycle in natural irradiance. *J. Geophys. Res.-Ocean*. **100,** 13295–13307 (1995).

44. Dall'Olmo, G., *et al.* Inferring phytoplankton carbon and eco-physiological rates from diel cycles of spectral particulate beam-attenuation coefficient. *Biogeosci.* **8,** 3423-3439 (2011).